CrystEngComm



PAPER

View Article Online

View Journal | View Issue



Cite this: CrystEngComm, 2025, 27,

Received 11th December 2024, Accepted 6th February 2025

DOI: 10.1039/d4ce01250j

rsc.li/crystengcomm

Fine-tuning of gas uptake and selectivity in a hexafluorozirconate pillared coordination network that features two porous phases†

Nathan C. Harvey-Reid, ¹D^a Hayley S. Scott, ^a Komal M. Patil, ¹D^a Naveen Kumar, ^c Colm Healy, ^{ab} Michael J. Zaworotko, ¹D^c Soumya Mukherjee ¹D*^c and Paul E. Kruger ¹D*^a

Hybrid coordination networks, sustained by divalent transition metal ions and a combination of organic and inorganic linker ligands, are an emerging class of physisorbents for adsorptive gas and vapour capture, especially under trace (\leq 1%) concentrations. Herein, we report a Cu(II) hybrid coordination network using the anionic pillar hexafluorozirconate ZrF₆²⁻, [Cu(pypz)₂ZrF₆I_n: ZRFSIX-21-Cu (21 = 4-(3,5-dimethyl-1*H*-pyrazol-4-yl)pyridine). ZRFSIX-21-Cu possesses two ultramicroporous phases, a two-dimensional square lattice phase (α), and a three-dimensional primitive cubic unit phase (β), a rarity among hybrid ultramicroporous materials. Interestingly, ZRFSIX-21-Cu- α revealed better selectivity for C₂H₂ over CO₂, and ZRFSIX-21-Cu- β for C₂H₂ over C₂H₄.

Introduction

Hybrid ultramicroporous materials (HUMs), ¹ a subfamily of hybrid coordination networks (HCNs), have emerged as a class of porous physisorbents suitable for gas separations. ¹⁻³ By taking advantage of ultramicroporous channels (<7 Å) and highly fluorinated pillars (SiF₆²⁻, TiF₆²⁻, *etc.*), HUMs offer strong electrostatic-rich high density of sorbate binding sites. Such strong binding often enables HUMs to demonstrate i) highly selective trace gas capture; ii) record-high binary and multicomponent gas separations (CO₂/N₂, C₂H₂/CO₂, C₂H₂/C₂H₄; C₂H₂/C₂H₄/CO₂, C₂H₂/C₂H₄/CH₄, among others). ^{2,4} Owing to their modular nature and amenability to the crystal engineering design principles, new HUMs can be readily synthesized. ⁵ Simply put, fine-tuning of components within the core blueprint of HUMs enables superior control of their pore environment. This is key to optimising the resulting

performance parameters,² such as gas uptake, binding

Traditionally, the above-mentioned HUMs relied upon pyrazine or pyridyl linkers to dictate pore size and/or promote interpenetration.⁷ The latest generation of HUMs have advanced this area by utilizing other N-heterocyclic derivatives, namely pyrazole. A recent report demonstrated the crystal engineering of a series of HUMs incorporating 4-(3,5-dimethyl-1*H*-pyrazol-4-yl) pyridine (pypz). ¹⁴ Inclusion of this ligand into the HUM platform afforded materials possessing both high selectivity and working capacity of C2H2 over CO2.15 Additionally, use of such ligands has been found to promote increased hydrolytic stability, which has been a prevalent issue in both HUMs and metal-organic materials (MOMs), in general. 16,17 Previous studies have shown that exposure to water or water vapour in HUMs typically leads to a structural transformation of the 3D pcu network to a 2D square lattice sql or sql-c* network. In the latter case, the square grids are interlocked, and the pillaring anions displaced, resulting in non-porous structures (Fig. 1). 17,18

To further explore the capabilities of the **pypz** ligand within a HUM platform, we report here the synthesis of $[Cu(pypz)_2ZrF_6]_n$ (**ZRFSIX-21-Cu**), a new HUM featuring the ZrF_6^{2-} pillar. Unlike its parent HUM, **SIFSIX-21-Cu**, ¹⁵ **ZRFSIX-**

energy, selectivity, and separation potential.^{6–8} To optimise these aspects, several iterations of HUMs have been synthesized, often by varying the inorganic pillaring linkers. These include the first and second generation HUMs, namely, **MFSIX** (SiF₆^{2–}, TiF₆^{2–}, GeF₆^{2–}),^{8,9} **DICRO** (Cr₂O₇^{2–}),¹⁰ **MOFFIVE** (NbOF₅^{2–}, TaOF₅^{2–}),¹¹ **MFFIVE** (AlF₅^{2–}, FeF₅^{2–}),¹² and the **mmo** nets (CrO₄^{2–}, MOO₄^{2–}, WO₄^{2–}).¹³

Traditionally, the above-mentioned HUMs relied upon

 ^a MacDiarmid Institute for Advanced Materials and Nanotechnology, School of Physical and Chemical Sciences, University of Canterbury, Private Bag 4800, Christchurch 8140, New Zealand. E-mail: paul.kruger@canterbury.ac.nz
 ^b Department of Chemistry, Harvey Mudd College, 301 Platt Blvd, Claremont, CA

b Department of Chemistry, Harvey Mudd College, 301 Platt Blvd, Claremont, CA 91711, USA
 c Department of Chemical Sciences, Bernal Institute and Research Ireland Centre

^{*}Department of Chemical Sciences, Bernal Institute and Research Ireland Centre for Pharmaceuticals (SSPC), University of Limerick, Limerick V94 T9PX, Ireland. E-mail: Soumya.Mukherjee@ul.ie

[†] Electronic supplementary information (ESI) available: Experimental details, syntheses and characterisations: infrared spectra, thermogravimetric traces, powder X-ray diffractograms, gas sorption isotherms, *etc.* CCDC deposition entries 2408456 and 2408457. For ESI and crystallographic data in CIF or other electronic format see DOI: https://doi.org/10.1039/d4ce01250j

CrystEngComm Paper

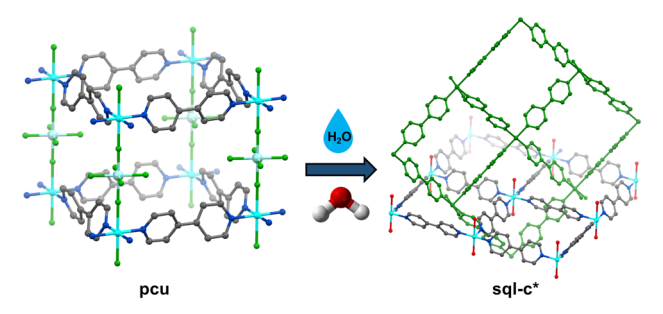


Fig. 1 Illustration showing the phase transition of a prototypical pcu topology HUM to an sql-c* topology CN, in the presence of excess water.

21-Cu exists in two distinct ultramicroporous phases, a 2D square lattice (sql) α-phase and a conventional 3D pillared pcu β-phase. Strikingly, and different to other anion-pillared HUMs, ZRFSIX-21-Cu is shown also to be porous in its 2D phase, a first in this family of materials. The work here reveals the structural differences between the phases and the impact these have on the porosity and separation potential for different gas mixtures.

Results and discussion

Synthesis and structural characterization

Single crystals of ZRFSIX-21-Cu-α were isolated following the evaporation of an acetonitrile solution containing a mixture of pypz, Cu2+ and ZrF62-, whereas single crystals of ZRFSIX-21-Cu-β were obtained through layering the reagents atop each other in methanol at room temperature. Bulk samples of the α-phase were synthesized directly by mixing the reagents in acetonitrile, whereas methanol solvent afforded the β -phase (see synthesis section of ESI† for further details). Single-crystal X-ray diffraction (SC-XRD) revealed that ZRFSIX-21-Cu-β is isostructural to the previously reported pypz-based HUMs (SIFSIX-21-Cu, SIFSIX-21-Ni, crystallising as a pcu topology framework in the orthorhombic space group Pnna. 15 Whereas ZRFSIX-21-Cu-α crystallises as an sql network in the orthorhombic space group Pna21, it can be characterised as an incomplete or intermediate phase in the formation of ZRFSIX-21-Cu-β. The key difference between the two phases is that ZRFSIX-21-Cu-α contains only one axially bound ZrF₆²⁻ anion per Cu²⁺ node, rather than two, resulting in a square pyramidal {N₄F} coordination chromophore around the Cu(II) centre (Fig. S1†). The absence of a second axial ZrF₆²⁻ anion in **ZRFSIX**-21-Cu-α leads to sequential sql layers exhibiting AB stacking, instead of being locked into a **pcu** network (Fig. S2†).

Ultramicroporosity is present in both phases due to onedimensional channels aligned along the crystallographic c-axis for α and b-axis for β , respectively. **ZRFSIX-21-Cu-\alpha** was found to feature a minimum pore window of ca. 2.5 Å, and a maximum pore window of ca. 6.0 Å (Fig. 2a and b). In ZRFSIX-21-Cu-β, the pore window was determined at ca. 4.8 Å, comparable to the isostructural HUM, SIFSIX-21-Cu (4.5

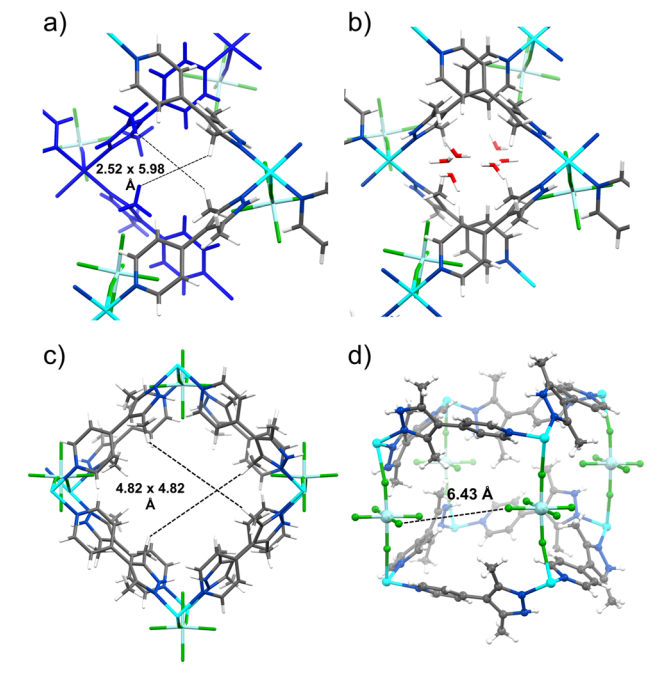


Fig. 2 Crystal structures of ZRFSIX-21-Cu (α and β). Ultramicropores of ZRFSIX-21-Cu-α generated through AB stacking of 2D layers. (b) Packing of the guest solvent molecules within the pores of ZRFSIX-21-Cu-α. (c) Ultramicropores of 3D ZRFSIX-21-Cu-β. (d) ZrF_6^{2-} pillars of ZRFSIX-21-Cu- β used to generate the 3D structure and to potentially facilitate strong sorbate binding sites (due to short F-F distances between the neighbouring pillars). Colour code: Cu (cyan), Zr (pale blue), F (green), N (blue), C (grey) and H (white).

Å), and TIFSIX-4-Cu (4.7 Å) (Fig. 2c). 15 Interestingly, the pore chemistry of **ZRFSIX-21-Cu-\alpha** resembles that of the previously reported sql HUM, sql-16-Cu-NO₃- α (16 = 4,4'-(2,5-dimethyl-1,4-phenylene)dipyridine).¹⁹ In both cases, the pore window is partially occupied by the coordinating anion, causing the axial anions to interdigitate between the undulating 2D layers. The presence of the NO_3^- anion in sql-16-Cu-NO₃- α contributed to strong sorbent-sorbate interactions observed for C₂H₂ compared with CO₂, ¹⁹ suggesting a similar effect might be observed with the ZrF_6^{2-} anion in **ZRFSIX-21-Cu-** α .

Powder X-ray diffraction (PXRD) was employed to confirm the bulk phase purity of ZRFSIX-21-Cu- α and β , as well as to verify the structural distinction between the two materials (sql vs. pcu). The PXRD diffractogram recorded after air drying revealed that ZRFSIX-21-Cu- α exists in a desolvated α' phase, as indicated by subtle differences between the simulated and experimental diffractograms. Thermogravimetric analysis (TGA) showed decomposition occurring at 473 K and 538 K for ZRFSIX-21-Cu- α and ZRFSIX-21-Cu- β , respectively (Fig. S5†).

Phase transition studies

To establish the relationship between and interconversion of **ZRFSIX-21-Cu-\alpha** and **ZRFSIX-21-Cu-\beta** phases, we conducted a

Paper

caries of experiments to track the transition between executes

series of experiments to track the transition between crystals of the α and β phases.

When soaked in a solution of MeOH, violet crystals of **ZRFSIX-21-Cu-** α were observed to slowly undergo a gradual phase transition to yield characteristic light-blue crystals of the **ZRFSIX-21-Cu-** β phase, over a period of 48 hours (Fig. S42†). PXRD measurements showed that in 24 hours, the sample comprised of a mixture of α and β phases, with complete conversion to **ZRFSIX-21-Cu-** β observed at 48 hours (Fig. 3). TGA measurements also confirmed successful phase transition as the decomposition profile complements that of the directly synthesized **ZRFSIX-21-Cu-** β (Fig. S5†). Attempts to reverse the phase change through heating crystals of **ZRFSIX-21-Cu-** β in acetonitrile or water to regenerate **ZRFSIX-21-Cu-** α were unsuccessful, suggesting thermodynamic stability of the β phase over the α phase.

Attempts were also made to induce a phase transition through direct heating of dried **ZRFSIX-21-Cu-\alpha** to remove any residual solvent and potentially enable the ${\rm ZrF_6}^2$ anions to lock the 2D layers together, forming **ZRFSIX-21-Cu-\beta**. These efforts were inspired by our previous work on the HUM **SIFSIX-3-Ni**, where the 3D material was realised by heating the **sql** precursor at 80 °C under vacuum. Heating **ZRFSIX-21-Cu-\alpha** at 120 °C under vacuum resulted in the formation of an additional poly-crystalline phase, **ZRFSIX-21-Cu-\alpha** (Fig. S6 and S8†), distinguishable by its green colour (Fig. 4). No phase transition was observed below 120 °C, with **ZRFSIX-21-Cu-\alpha** remaining unchanged.

Gas adsorption studies

Single-component gas adsorption studies were conducted on all three phases to evaluate their porosity. Activation of ZRFSIX-21-Cu- α at 50 °C and 120 °C under vacuum generated the phases ZRFSIX-21-Cu- α and ZRFSIX-21-Cu- γ (Fig. S6†), while ZRFSIX-21-Cu- β was activated at room temperature under vacuum. N₂ adsorption isotherms at 77 K revealed that

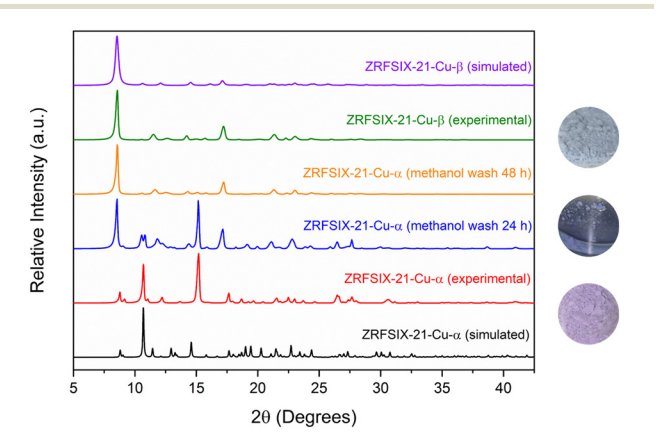


Fig. 3 PXRD patterns of ZRFSIX-21-Cu. ZRFSIX-21-Cu- α (red) undergoes a phase transition to ZRFSIX-21-Cu- β (green) upon treatment with methanol, over a 48 hour period (blue and yellow). Optical images on the right illustrate colour change observed during the α to β phase transition.

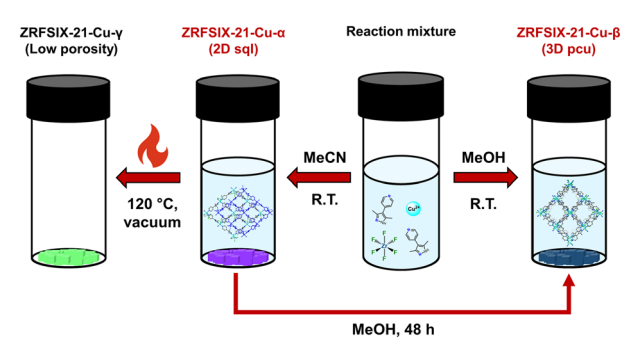


Fig. 4 Reaction pathways for the synthesis of ZRFSIX-21-Cu- α , ZRFSIX-21-Cu- β and ZRFSIX-21-Cu- γ .

both ZRFSIX-21-Cu-α' and ZRFSIX-21-Cu-β displayed typical type I isotherms, with BET surface areas calculated at 367 m² g⁻¹ and 404 m² g⁻¹, respectively, whereas **ZRFSIX-21-Cu-**γ showed no N2 uptake (Fig. S9, S18 and S25†). Since ZRFSIX-21-Cu-y was subjected to harsh activation at 120 °C under high vacuum, quality of the single crystals was no longer suitable for SC-XRD studies. Notably, the surface area of ZRFSIX-21-Cu-β was found to be markedly reduced compared to the other pypz-based HUMs, which typically report surface areas ranging from 747 m² g⁻¹ to 931 m² g⁻¹. ¹⁴ CO₂ isotherms at 195 K showed similar uptake levels and pore size distributions in ZRFSIX-21-Cu-α' and ZRFSIX-21-Cu-β (Fig. S9 and S18†), whereas ZRFSIX-21-Cu-y exhibited lower CO2 uptake at 195 K, resulting in a BET surface area of 343 m² g⁻¹ (Fig. S25†). In ZRFSIX-21-Cu-γ, the lack of N2 uptake and minimal CO₂ uptake at 195 K were further supported by no uptake observed across several other gas isotherms at 298 K (Fig. S26-S29†). The conspicuously low BET surface areas of **ZRFSIX-21-Cu-\alpha'** and **ZRFSIX-21-Cu-\beta**, relative to other pypzbased HUMs, prompted us to explore their ability to adsorb CO₂ and C₂ gases under ambient conditions. C₂H₂, C₂H₄, and CO₂ adsorption isotherms were measured at 273, 283, and 298 K for ZRFSIX-21-Cu-α' and at 273 and 298 K for ZRFSIX-21-Cu-β. All measurements recorded at 273 K and above displayed type I isotherms.

ZRFSIX-21-Cu-α' at ambient temperatures

At 1 bar and 298 K, the C_2H_2 uptake was 57.0 cm³ g⁻¹, while the CO_2 uptake was less than half this value, at 24.2 cm³ g⁻¹ (Fig. 5a).

The C_2H_2/CO_2 uptake ratio for **ZRFSIX-21-Cu-\alpha'** was calculated to be 2.4, comparable to previously reported **sql** networks **UTSA-83a** $(3.1)^{20}$ and **sql-16-Cu-NO₃-\alpha'** (2.1). Although it has a lower uptake ratio, **ZRFSIX-21-Cu-\alpha'** exhibits a much higher C_2H_2 uptake capacity, nearly five times that of **UTSA-83a** $(57.0 \text{ cm}^3 \text{ g}^{-1} \text{ vs. } 11.9 \text{ cm}^3 \text{ g}^{-1})$. The isosteric enthalpies of adsorption (Q_{st}) for C_2H_2 and CO_2 were determined from the isotherms at 273, 283, and 298 K. Lowloading Q_{st} values for C_2H_2 $(32.0 \text{ kJ mol}^{-1})$ and CO_2 $(22.8 \text{ kJ mol}^{-1})$ were consistent with the significant difference in pure gas isotherm uptakes (Fig. 5c and S30†).

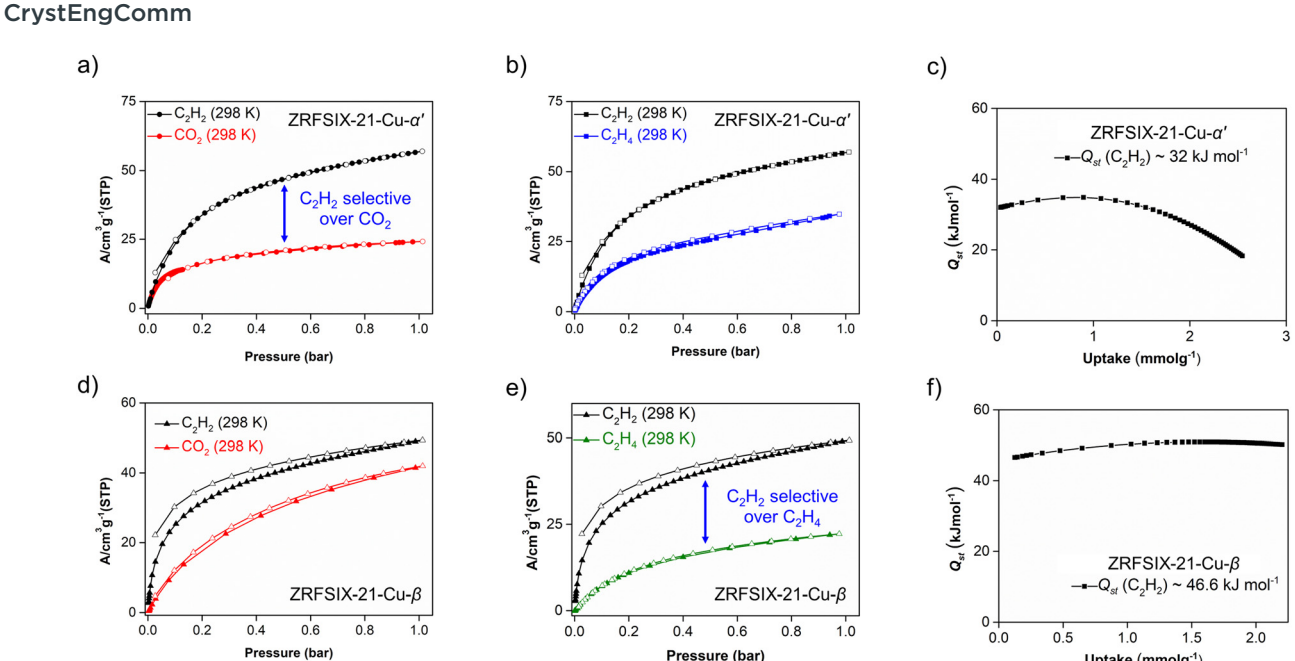


Fig. 5 Adsorption isotherms of ZRFSIX-21-Cu- α' for (a) C₂H₂ and CO₂ at 298 K and (b) C₂H₂ and C₂H₄ at 298 K. Closed and open symbols represent adsorption and desorption, respectively. (c) C₂H₂ adsorption enthalpy for ZRFSIX-21-Cu- α' . Adsorption isotherms of ZRFSIX-21-Cu- β for (d) C₂H₂ and CO₂ at 298 K and (e) C₂H₂ and C₂H₄ at 298 K respectively. (f) C₂H₂ adsorption enthalpy for ZRFSIX-21-Cu- β .

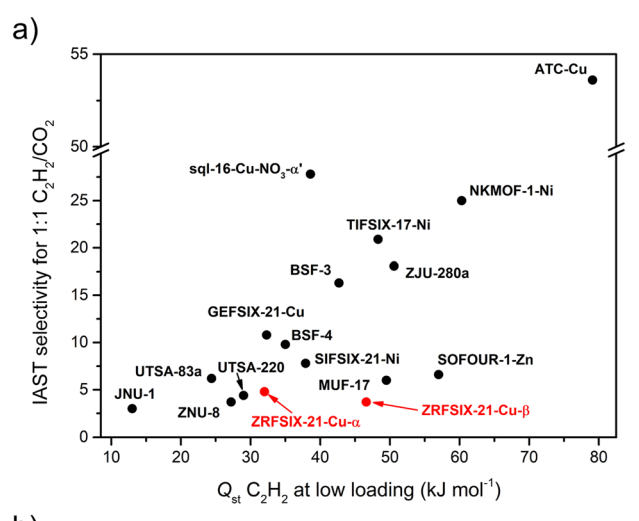
The selectivity of C₂H₂/CO₂ was determined using IAST by fitting the pure gas isotherms to the dual-site Langmuir-Freundlich equation. For a binary mixture of C₂H₂/CO₂ (1:1, v/v) at 1 bar and 298 K, the selectivity of C₂H₂/CO₂ was 4.8 (Fig. S34†), which is lower than that of sql-16-Cu-NO₃- α' $(27.8)^{19}$ and **UTSA-83a** $(6.2)^{20}$ yet still higher than several 3D C_2H_2 adsorbents such as UTSA-220 (4.4), ²¹ FJU-89a (4.3), ²² ZNU-8 (3.7),²³ JNU-1 (3.0),²⁴ and Zn-MOF-74 (2.0) (Fig. 6a).²⁵ Notably, at 1 bar and 283 K, the selectivity of **ZRFSIX-21-Cu-** α' increases significantly to 15.2, suggesting more favourable conditions for C₂H₂/CO₂ separation. With its relatively low binding energy and high C₂H₂ capacity, ZRFSIX-21-Cu-α' demonstrates potential as a versatile, C2H2-selective sorbent, with implications for mild regeneration conditions. Adsorption isotherms for C2H4 were also collected for **ZRFSIX-21-Cu-\alpha'**, showing an uptake of 34.8 cm³ g⁻¹ at 1 bar and 298 K and a C₂H₂/C₂H₄ uptake ratio of 1.6 (Fig. 5b). However, similar Q_{st} values for C₂H₂ (32.0 kJ mol⁻¹) and C₂H₄ (30.7 kJ mol⁻¹) (Fig. 5c and S31†), along with a low selectivity of 1.7 (1:1, v/v), indicated that **ZRFSIX-21-Cu-** α' is not wellsuited for C₂H₂/C₂H₄ separation (Fig. S34†).

ZRFSIX-21-Cu-β at ambient temperatures

As observed in isostructural analogues, **ZRFSIX-21-Cu-\beta** also demonstrated a higher affinity for C_2H_2 over CO_2 , with uptakes of 49.4 cm³ g⁻¹ and 42.0 cm³ g⁻¹ at 1 bar and 298 K, respectively (Fig. 5d), and a significantly lower C_2H_4 uptake of 22.2 cm³ g⁻¹ (Fig. 5e). Although the C_2H_2/CO_2 uptake ratio for **ZRFSIX-21-Cu-\beta** is lower than that of **ZRFSIX-21-Cu-\alpha** (1.2 ν s. 2.4), **ZRFSIX-21-Cu-\beta** exhibited superior uptake kinetics for C_2H_2 relative to CO_2 . Calculated Q_{st} values revealed

binding energies of 46.6 and 28.3 kJ mol⁻¹ for C₂H₂ and CO₂ at zero loading, respectively (Fig. 5f and S32†). Compared to ZRFSIX-21-Cu-α', ZRFSIX-21-Cu-β exhibits a much greater affinity for C₂H₂, with a difference of 14.6 kJ mol⁻¹ in their C₂H₂ binding energies, while the CO₂ values remain relatively similar. This change in Q_{st} is likely due to differences in the pore environment between the α and β phases. Considering Q_{st} values at half-loading, an important metric for assessing 1:1 C₂H₂/CO₂ separations, the binding energy difference $(\Delta Q_{\rm st})_{\rm C,H,/CO_3}$ for **ZRFSIX-21-Cu-\beta** increases substantially to 28.5 kJ mol⁻¹. This $(\Delta Q_{\rm st})_{\rm C_2H,/CO_2}$ value exceeds those of many high-performing C2H2/CO2 selective materials, such as the TCuX series (X: Br, Cl, I; 5.5-8.2 kJ mol⁻¹), 26 UTSA-74a (6.0 kJ mol^{-1}),²⁷ **NKMOF-1-Ni** (9.5 kJ mol^{-1}),²⁸ and **sql-16-Cu-NO**₃- α' (11.4 kJ mol⁻¹).¹⁹ Only benchmark materials such as ATC-Cu exhibit a greater $(\Delta Q_{\rm st})_{\rm C_2H_2/CO_3}$ at half-loading, a value heavily influenced by its exceptionally high binding energy for C2H2 $(Q_{\rm st} = 79.1 \text{ kJ mol}^{-1}).^{29}$

As shown in previous studies of isostructural HUMs (e.g., SIFSIX-21-Ni, SIFSIX-21-Cu), ¹⁵ ZRFSIX-21-Cu- β benefits from multiple ZrF₆²⁻ pillars and methyl groups that line the walls of the material. These features create strong electrostatic binding sites within the HUM, effectively trapping acetylene. ZRFSIX-21-Cu- α ′ can be considered an "incomplete" phase of ZRFSIX-21-Cu- β . SC-XRD analysis reveals that the ZrF₆ anions bound in ZRFSIX-21-Cu- α ′ are isolated from neighbouring ZrF₆²⁻ anions due to the interdigitation of sql layers, which could significantly reduce the effectiveness of the binding sites, limiting C₂H₂ interactions to a single ZrF₆²⁻ pillar and weaker interactions with the ligand. Furthermore, the larger ZrF₆²⁻ anion in ZRFSIX-21-Cu- β results in a greater



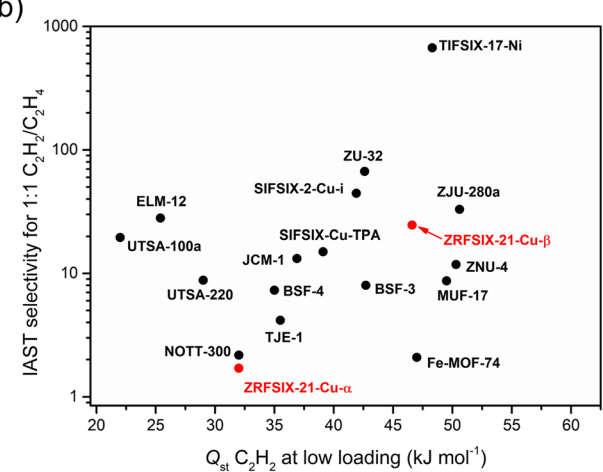


Fig. 6 Comparison scatter plot of C_2H_2 heat of adsorption and IAST selectivity for a) C_2H_2/CO_2 (1:1) and b) C_2H_2/C_2H_4 (1:1) of ZRFSIX-21-Cu-α and ZRFSIX-21-Cu-β with other top performing sorbents at 298 K. Molecular sieving materials have been omitted for clarity.

protrusion of F atoms into the pore windows due to longer Zr–F bonds (2.015 Å) and short F–F distances (6.43 Å) between adjacent ${\rm ZrF_6}^{2^-}$ pillars (Fig. 2d), leading to a contracted pore volume and enhanced binding between sorbent and sorbate. IAST selectivity calculations for 1:1 binary mixture confirmed $S_{\rm C_2H_2/CO_2}$ and $S_{\rm C_2H_2/C_2H_4}$ values of 3.7 and 24.6 at 1 bar and 298 K, respectively (Fig. S35†), with ${\rm C_2H_2/CO_2}$ selectivity comparable to **ZRFSIX-21-Cu-** α' ($S_{\rm C_2H_2/CO_2}$ (1:1) = 4.8). With a selectivity of 24.6, **ZRFSIX-21-Cu-** β is well-suited for ${\rm C_2H_2/C_2H_4}$ separation. However, these values still lag a few HUM physisorbents and other materials (Fig. 6b), such as the benchmark material **ZJU-300a.** Additionally, **SIFSIX-14-Cu-i** and **UTSA-300a** exploit molecular sieving to achieve record-high selectivities.

Conclusions

Ultramicroporous materials **ZRFSIX-21-Cu-** α , with a **sql** topology, and **ZRFSIX-21-Cu-** β , with a **pcu** topology, are additions to the MFSIX series of sorbents. Although they

share an identical chemical formula, they form distinct structures due to variations in the $Cu(\pi)$ coordination geometry and can be synthesised separately depending on the reaction conditions. Gas adsorption analysis revealed that both α and β phases are selective for C_2H_2 , though unexpectedly, each favours a different gas pair. The α phase is more selective for C_2H_2 over CO_2 , while the β phase shows higher selectivity for C_2H_2 over C_2H_4 . Notably, IAST calculations indicate that **ZRFSIX-21-Cu-\beta** exhibits excellent C_2H_2/C_2H_4 selectivity (24.6). These newly discovered materials as physisorbents exemplify the nuances of crystal engineering and underscore the value of tuneable phases for specific gas separations.

Data availability

The data supporting this article have been included as part of the ESI.† Crystallographic data for **ZRFSIX-21-Cu-\alpha** and **ZRFSIX-21-Cu-\beta** can be accessed from the Cambridge Crystallographic Data Centre (CCDC) as deposition numbers 2408456 and 2408457, respectively.

Author contributions

Conceptualization, N. C. H. R., S. M., M. J. Z., and P. E. K.; methodology, N. C. H. R., H. S. S. and K. M. P.; investigation, N. C. H. R., H. S. S., K. M. P., N. K. and S. M.; formal analysis, N. C. H. R., K. M. P., N. K., C. H., S. M. and P. E. K.; data curation, N. C. H. R., K. M. P., N. K., C. H., S. M. and P. E. K.; writing – original draft, N. C. H. R., S. M. and P. E. K.; writing – review & editing, all authors; funding acquisition, S. M., M. J. Z., and P. E. K.; supervision, S. M. and P. E. K.

Conflicts of interest

There are no conflicts to declare.

Acknowledgements

This publication arises from research supported by Research Ireland (formerly known as the Science Foundation Ireland) awarded to S. M., under grant number 21/PATH-S/9454. For open access, the authors have applied a CC BY public copyright licence to any author-accepted manuscript version of this submission. M. J. Z. and S. M. thank the SSPC Reward funding, AzAds. P. E. K. gratefully acknowledges the MacDiarmid Institute for Advanced Materials and Nanotechnology, and the School of Physical and Chemical Science at the University of Canterbury for financial and instrumental support.

Notes and references

- 1 S. Mukherjee and M. J. Zaworotko, *Trends Chem.*, 2020, 2, 506–518.
- 2 (a) S. Mukherjee, D. Sensharma, K.-J. Chen and M. J. Zaworotko, Chem. Commun., 2020, 56, 10419–10441; (b) X.

CrystEngComm Paper

- Liu, H. Wang, C. Liu, J. Chen, Z. Zhou, S. Deng and J. Wang, Chem Bio Eng., 2024, 1(6), 469-487.
- 3 (a) Z. Ajoyan, P. Marino and A. J. Howarth, CrystEngComm, 2018, 20, 5899-5912; (b) T. Wang, E. Lin, Y.-L. Peng, Y. Chen, P. Cheng and Z. Zhang, Coord. Chem. Rev., 2020, 423, 213485; (c) J. Dechnik, J. Gascon, C. J. Doonan, C. Janiak and C. J. Sumby, Angew. Chem., Int. Ed., 2017, 56, 9292-9310; (d) S. J. Datta, A. Mayoral, N. M. S. Bettahalli, P. M. Bhatt, M. Karunakaran, I. D. Carja, D. Fan, M. M. P. Graziane, R. Semino, G. Maurin, O. Terasaki and M. Eddaoudi, Science, 2022, 376, 1080-1087.
- 4 (a) X. Li, H. Bian, W. Huang, B. Yan, X. Wang and B. Zhu, Coord. Chem. Rev., 2022, 470, 214714; (b) Y. Jiang, W. Yang, Y. Zhang, L. Wang and B. Chen, J. Mater. Chem. A, 2024, 12, 5563-5580.
- 5 (a) S. Subramanian and M. J. Zaworotko, Angew. Chem., Int. Ed. Engl., 1995, 34, 2127-2129; (b) W. Lu, Z. Wei, Z.-Y. Gu, T.-F. Liu, J. Park, J. Park, J. Tian, M. Zhang, Q. Zhang, T. Gentle, M. Bosch and H.-C. Zhou, Chem. Soc. Rev., 2014, 43, 5561-5593.
- 6 (a) K. Uemura, A. Maeda, T. K. Maji, P. Kanoo and H. Kita, Eur. J. Inorg. Chem., 2009, 16, 2329-2333; (b) P. Nugent, Y. Belmabkhout, S. D. Burd, A. J. Cairns, R. Luebke, K. Forrest, T. Pham, S. Ma, B. Space, L. Wojtas, M. Eddaoudi and M. J. Zaworotko, Nature, 2013, 495, 80; (c) S. K. Elsaidi, M. H. Mohamed, H. T. Schaef, A. Kumar, M. Lusi, T. Pham, K. A. Forrest, B. Space, W. Xu, G. J. Halder, J. Liu, M. J. Zaworotko and P. K. Thallapally, Chem. Commun., 2015, 51, 15530-15533.
- 7 A. Ebadi Amooghin, H. Sanaeepur, R. Luque, H. Garcia and B. Chen, Chem. Soc. Rev., 2022, 51, 7427-7508.
- 8 X. Cui, K. Chen, H. Xing, Q. Yang, R. Krishna, Z. Bao, H. Wu, W. Zhou, X. Dong, Y. Han, B. Li, Q. Ren, M. J. Zaworotko and B. Chen, Science, 2016, 353, 141-144.
- 9 S.-i. Noro, S. Kitagawa, M. Kondo and K. Seki, Angew. Chem., Int. Ed., 2000, 39, 2081-2084.
- 10 (a) H. S. Scott, N. Ogiwara, K.-J. Chen, D. G. Madden, T. Pham, K. Forrest, B. Space, S. Horike, J. J. Perry IV, S. Kitagawa and M. J. Zaworotko, Chem. Sci., 2016, 7, 5470-5476; (b) H. S. Scott, S. Mukherjee, D. R. Turner, M. I. J. Polson, M. J. Zaworotko and P. E. Kruger, CrystEngComm, 2018, 20, 1193-1197.
- 11 (a) A. Cadiau, K. Adil, P. M. Bhatt, Y. Belmabkhout and M. Eddaoudi, Science, 2016, 353, 137-140; (b) B. Gao, Z. Zhang, J. Hu, L. Yang, Y. Li, L. Chen, X. Cui and H. Xing, Chin. J. Chem. Eng., 2022, 42, 49-54.
- 12 A. Cadiau, Y. Belmabkhout, K. Adil, P. M. Bhatt, R. S. Pillai, A. Shkurenko, C. Martineau-Corcos, G. Maurin and M. Eddaoudi, Science, 2017, 356, 731-735.
- 13 M. H. Mohamed, S. K. Elsaidi, T. Pham, K. A. Forrest, H. T. Schaef, A. Hogan, L. Wojtas, W. Xu, B. Space, M. J. Zaworotko and P. K. Thallapally, Angew. Chem., Int. Ed., 2016, 55, 8285-8289.

- 14 N. Kumar, S. Mukherjee, N. C. Harvey-Reid, A. A. Bezrukov, K. Tan, V. Martins, M. Vandichel, T. Pham, L. M. van Wyk, K. Oyekan, A. Kumar, K. A. Forrest, K. M. Patil, L. J. Barbour, B. Space, Y. Huang, P. E. Kruger and M. J. Zaworotko, Chem, 2021, 7, 3085-3098.
- 15 N. C. Harvey-Reid, D. Sensharma, S. Mukherjee, K. M. Patil, N. Kumar, S. J. Nikkhah, M. Vandichel, M. J. Zaworotko and P. E. Kruger, ACS Appl. Mater. Interfaces, 2024, 16, 4803-4810.
- 16 A. J. Howarth, Y. Liu, P. Li, Z. Li, T. C. Wang, J. T. Hupp and O. K. Farha, Nat. Rev. Mater., 2016, 1, 15018.
- 17 D. O'Nolan, A. Kumar and M. J. Zaworotko, J. Am. Chem. Soc., 2017, 139, 8508-8513.
- 18 D. Sensharma, S. Vaesen, C. Healy, J. Hartmann, A. C. Kathalikkattil, P. Wix, F. Steuber, N. Zhu and W. Schmitt, Eur. J. Inorg. Chem., 2018, 2018, 1993-1997.
- 19 N. Kumar, S. Mukherjee, A. A. Bezrukov, M. Vandichel, M. Shivanna, D. Sensharma, A. Bajpai, V. Gascón, K. Otake and S. Kitagawa, SmartMat, 2020, 1, e1008.
- 20 H. Cui, S. Chen, H. Arman, Y. Ye, A. Alsalme, R.-B. Lin and B. Chen, Inorg. Chim. Acta, 2019, 495, 118938.
- 21 H. Li, L. Li, R.-B. Lin, G. Ramirez, W. Zhou, R. Krishna, Z. Zhang, S. Xiang and B. Chen, ACS Sustainable Chem. Eng., 2019, 7, 4897-4902.
- 22 Y. Ye, S. Chen, L. Chen, J. Huang, Z. Ma, Z. Li, Z. Yao, J. Zhang, Z. Zhang and S. Xiang, ACS Appl. Mater. Interfaces, 2018, 10, 30912-30918.
- 23 Y. Zhang, W. Sun, B. Luan, J. Li, D. Luo, Y. Jiang, L. Wang and B. Chen, Angew. Chem., Int. Ed., 2023, 62, e202309925.
- 24 H. Zeng, M. Xie, Y. Huang, Y. Zhao, X. Xie, J. Bai, M. Wan, R. Krishna, W. Lu and D. Li, Angew. Chem., Int. Ed., 2019, 58, 8515-8519.
- 25 S. Xiang, W. Zhou, Z. Zhang, M. A. Green, Y. Liu and B. Chen, Angew. Chem., Int. Ed., 2010, 49, 4615-4618.
- 26 S. Mukherjee, Y. He, D. Franz, S. Wang, W. Xian, A. A. Bezrukov, B. Space, Z. Xu, J. He and M. J. Zaworotko, Chem. - Eur. J., 2020, 26, 4923-4929.
- 27 F. Luo, C. Yan, L. Dang, R. Krishna, W. Zhou, H. Wu, X. Dong, Y. Han, T.-L. Hu and M. O'Keeffe, J. Am. Chem. Soc., 2016, 138, 5678-5684.
- 28 Y.-L. Peng, T. Pham, P. Li, T. Wang, Y. Chen, K.-J. Chen, K. A. Forrest, B. Space, P. Cheng, M. J. Zaworotko and Z. Zhang, Angew. Chem., Int. Ed., 2018, 57, 10971-10975.
- 29 Z. Niu, X. Cui, T. Pham, G. Verma, P. C. Lan, C. Shan, H. Xing, K. A. Forrest, S. Suepaul, B. Space, A. Nafady, A. M. Al-Enizi and S. Ma, Angew. Chem., Int. Ed., 2021, 60, 5283-5288.
- 30 X. W. Gu, E. Wu, J. X. Wang, H. M. Wen, B. Chen, B. Li and G. Qian, Sci. Adv., 2023, 9, eadh0135.
- 31 B. Li, X. Cui, D. O'Nolan, H.-M. Wen, M. Jiang, R. Krishna, H. Wu, R.-B. Lin, Y.-S. Chen, D. Yuan, H. Xing, W. Zhou, Q. Ren, G. Qian, M. J. Zaworotko and B. Chen, Adv. Mater., 2017, 29, 1704210.
- 32 R.-B. Lin, L. Li, H. Wu, H. Arman, B. Li, R.-G. Lin, W. Zhou and B. Chen, J. Am. Chem. Soc., 2017, 139, 8022-8028.